Nano Energy 39 (2017) 539–545

Contents lists available at ScienceDirect

Nano Energy

journal homepage: www.elsevier.com/locate/nanoen

Full paper

Well-designed Te/SnS_2/Ag artificial nanoleaves for enabling and enhancing visible-light driven overall splitting of pure water

Changzeng Yan[a,1], Xiaolan Xue[a,1], Wenjun Zhang[a,1], Xiaojie Li[a], Juan Liu[b], Songyuan Yang[a], Yi Hu[a], Renpeng Chen[a], Yaping Yan[c], Guoyin Zhu[a], Zhenhui Kang[b,*], Dae Joon Kang[c,*], Jie Liu[a,d,**], Zhong Jin[a,*]

[a] Key Laboratory of Mesoscopic Chemistry of MOE, School of Chemistry and Chemical Engineering, Nanjing University, Nanjing 210023, China
[b] Jiangsu Key Laboratory for Carbon-based Functional Materials and Devices, Institute of Functional Nano and Soft Materials (FUNSOM), Soochow University, Suzhou 215123, China
[c] Department of Interdisciplinary of Physics and Chemistry, Sungkyunkwan University, Suwon 440-746, South Korea
[d] Department of Chemistry, Duke University, Durham, NC 27708, USA

ARTICLE INFO

Keywords:
Overall water splitting
Visible-light driven
Artificial nanoleaves
P-n junctions
Surface plasmon resonance enhancement

ABSTRACT

To produce hydrogen and oxygen from photocatalytic overall splitting of pure water provides a promising green route to directly convert solar energy to clean fuel. However, the design and fabrication of high-efficiency photocatalyst is challenging. Here we present that by connecting different nanostructures together in a rational fashion, components that cannot individually split water into H_2 and O_2 can work together as efficient photocatalyst with high solar-to-hydrogen (STH) energy conversion efficiency and avoid the use of any sacrificial reagent. Specifically, Te/SnS_2/Ag artificial nanoleaves (ANLs) consist of ultrathin SnS_2 nanoplates grown on Te nanowires and decorated with numerous Ag nanoparticles. The appropriate band structure of Te/SnS_2 p-n junctions and the surface plasmon resonance of Ag nanoparticles synergistically enhance the quantum yield and separation efficiency of electron-hole pairs. As a result, Te/SnS_2/Ag ANLs enable visible-light driven overall water-splitting without any sacrificial reagent and exhibit high H_2 and O_2 production rates of 332.4 and 166.2 μmol h^{-1}, respectively. Well-preserved structure after long-term measurement indicates its high stability. It represents a feasible approach for direct H_2 production from only sunlight, pure water, and rationally-designed ANL photocatalysts.

1. Introduction

Solar-driven photocatalytic overall water-splitting offers an attractive approach for affordable and clean production of hydrogen [1–3]. However, it is still a long-standing challenge to develop advanced photocatalysts to generate H_2 with high energy-conversion efficiency and long-term stability. An ideal photocatalyst should be inexpensive, earth-abundant, non-toxic and can split water with high efficiency without the assistance of any sacrificial reagent.

Typically, photocatalytic water-splitting involves three stages: 1) light absorption; 2) electron-hole pair generation and separation; and 3) surface redox reactions. Over the past decades, lots of semiconductive photocatalysts have been carefully studied (such as TiO_2 [4,5], α-Fe_2O_3 [6,7], CdS [8,9], and C_3N_4 [10,11]). However, the efficiency of photocatalysts often suffers from narrow light absorption, low quantum yield, poor charge transport and slow interfacial kinetics, thus not propitious to effective light utilization and H_2 generation. To overcome these problems, various strategies have been developed, for examples, tuning of compositions (*e.g.* doping) and band gap engineering [12,13], construction of favorable nanostructures [12,14] and loading of co-catalysts or sensitizers (*e.g.* chalcogenides, dyes or metal nanoparticles) [15–17]. Newly-emerged semiconductor heterojunctions composed of versatile nanomaterials have attracted growing interest for water-splitting owing to their extraordinary properties and synergistic effect [2,16–18]. Nevertheless, the rational design of visible-light sensible photocatalysts that can efficiently split water into H_2 and O_2 without adding any sacrificial reagent still remains a great challenge (as detailed in Table S1, Supporting information).

Herein, we report novel Te/SnS_2/Ag artificial nanoleaves (ANLs) composed of three carefully-selected components with different

* Corresponding authors.
** Corresponding author at: Department of Chemistry, Duke University, Durham, NC 27708, USA.
E-mail addresses: zhkang@suda.edu.cn (Z. Kang), djkang@skku.edu (D.J. Kang), j.liu@duke.edu (J. Liu), zhongjin@nju.edu.cn (Z. Jin).
[1] These authors contributed equally.

http://dx.doi.org/10.1016/j.nanoen.2017.07.039
Received 7 March 2017; Received in revised form 17 July 2017; Accepted 23 July 2017
Available online 25 July 2017

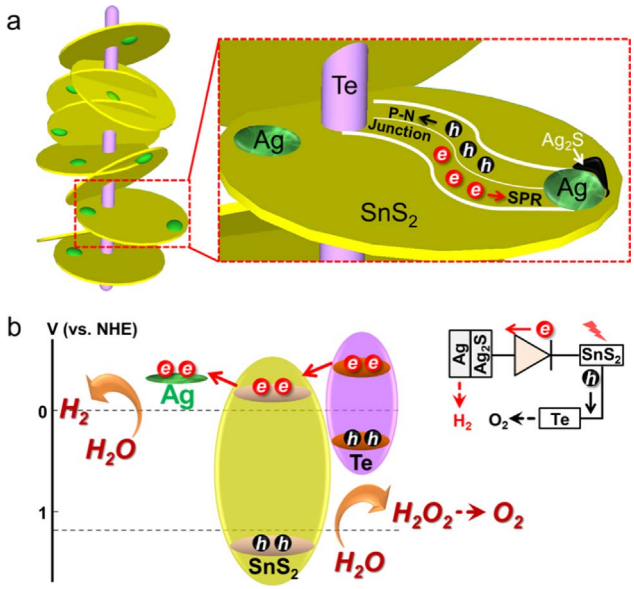

Scheme 1. (a) Schematic of the structure and components of Te/SnS_2/Ag ANLs. (b) Illustration of the charge separation and transport routes in Te/SnS_2/Ag ANLs.

characteristics and good synergistic effect as a high-performance photocatalyst (Scheme 1). Te nanowire, a p-type semiconductor with high conductivity [19] served as the branch of Te/SnS_2/Ag ANLs, and also enabled fast charge transport. Numerous SnS_2 nanoplates (n-type semiconductor with preferable edge-state position) [20,21] were grown on the Te nanowire for the construction of p-n junctions. Moreover, Ag nanoparticles were decorated on the surface of SnS_2 nanoplates as electron collectors and surface plasmon resonance (SPR) sources [22]. In this way, a "highway" made of "Te nanowire–SnS_2 nanoplates–Ag nanoparticles" was built in Te/SnS_2/Ag ANLs for efficient light utilization and charge separation, therefore enabled and improved visible-light driven splitting of pure water without any sacrificial reagent.

2. Experimental section

2.1. Preparation of Te nanowires

Te nanowires were synthesized *via* a modified hydrothermal reduction process.[S1] Briefly, 0.1 g sodium tellurite (Na_2TeO_3, Sigma-Aldrich) and 0.2 g polyvinyl pyrrolidone (PVP, Sinopharm Chemical) were dissolved in 100 mL deionized water. Subsequently, 1.0 mL of hydrazine hydrate ($N_2H_4{\cdot}H_2O$, Sinopharm Chemical) and 2.0 mL of ammonia water (25–28 wt% of NH_3, Sinopharm Chemical) were dropped into the solution under vigorous stirring in the dark. The above solution was transferred and sealed into a Teflon-lined autoclave. The autoclave was heated to 180 °C at a ramp rate of 5 °C min^{-1} and kept at this temperature for 3 h. Then the autoclave was cooled down naturally to room temperature. The product was centrifugated and washed sequentially by 50 mL of ethanol and water to remove any possible contaminations, and finally dried at 50 °C in a vacuum oven.

2.2. Preparation of Te/SnS_2 ANLs

In brief, 40 mg of above-prepared Te nanowires, 20 mg of thiourea (CH_4N_2S, Sinopharm Chemical) and 0.27 g of $SnCl_4{\cdot}5H_2O$ (Sinopharm Chemical) were sequentially added into 30 mL of ethylene glycol. The

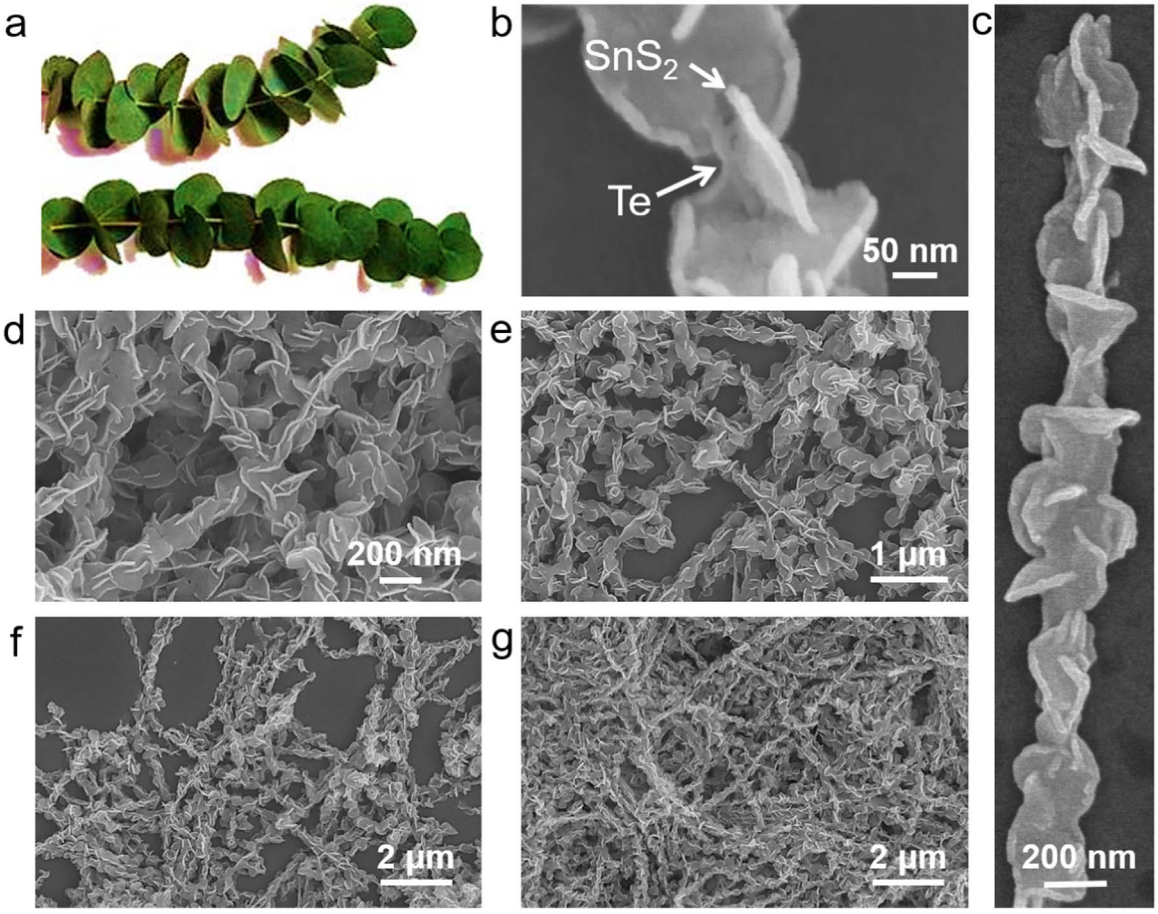

Fig. 1. (a) Photograph of tree leaves. (b-g) SEM images of Te/SnS_2/Ag ANLs at different magnifications, including an individual Te/SnS_2/Ag ANLs shown in (c).

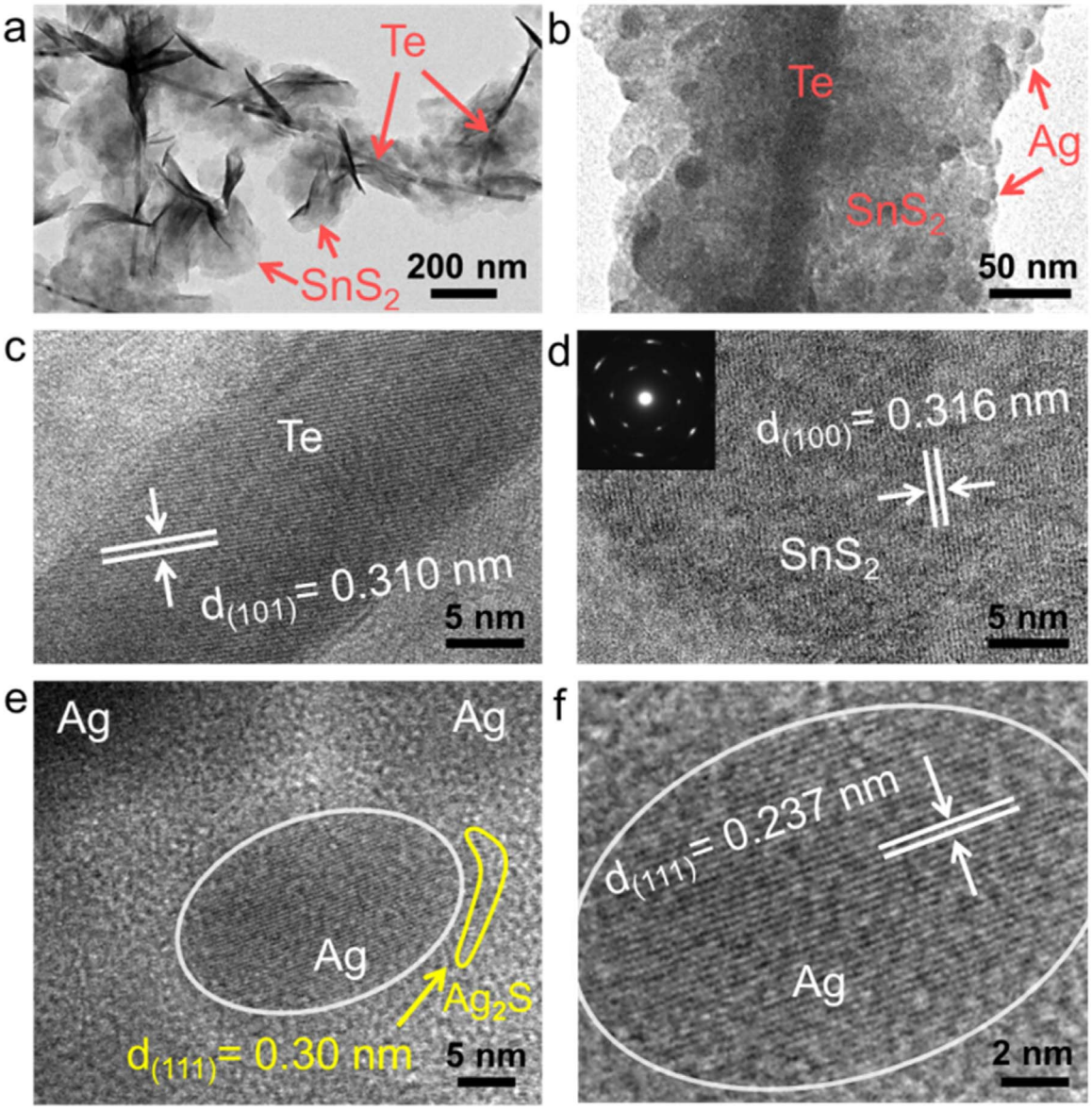

Fig. 2. (a) TEM image of Te/SnS_2/Ag ANLs. (b) TEM image showing Ag nanoparticles decorated on a SnS_2 nanoplate in Te/SnS_2/Ag ANLs. HRTEM images of (c) a Te nanowire and (d) a SnS_2 nanoplate in Te/SnS_2/Ag ANLs. The SAED pattern in the insert of (c) reveals its crystalline structure. (e) HRTEM image of Ag nanoparticles along with concomitantly-formed Ag_2S nanodots on SnS_2 nanoplates in Te/SnS_2/Ag ANLs. (f) The further magnification of (e).

solution was ultrasonicated with a cell crusher (JY92-IIDN, Ningbo Scientz) for 5 min and then transferred into a Teflon-lined stainless autoclave. The autoclave was heated at 180 °C for 12 h and then cooled to room temperature naturally. The obtained Te/SnS_2 ANLs was centrifugated and washed thoroughly with 50 mL ethanol and deionized water, and then dried in ambient air.

2.3. Preparation of Te/SnS_2/Ag ANLs

Simply, 50 mg of above-obtained Te/SnS_2 ANLs and 10 mg of silver nitrate ($AgNO_3$) were dissolved in 100 mL deionized water and ultrasonicated for 5 min. The solution was exposed under a Xe lamp (300 W, CEL-HXF300E, CEAULIGHT) for 10 min to decorate Ag nanoparticles on the surface of ANLs, thus realizing the formation of Te/SnS_2/Ag ANLs. The product was centrifugated and washed with 50 mL ethanol and deionized water sequentially and dried at 70 °C for 3 h.

2.4. Preparation of pristine SnS_2 nanoplates and decoration of Ag nanoparticles

The process for preparing pristine SnS_2 nanoplates is similar to the preparation of Te/SnS_2 ANLs, but without the addition of any Te nanowires. The approach to prepare SnS_2/Ag by decorating Ag nanoparticles on SnS_2 nanoplates is identical to the approach for decorating of Ag nanoparticles on Te/SnS_2 ANLs.

2.5. Characterizations

The samples were analyzed by scanning electron microscopy (SEM, Hitachi S-4800), high-resolution transmission electron microscopy (HRTEM, JEM-2100F), UV–Vis spectroscopy (Shimadzu UV-2600 spectrometer) and X-ray diffraction (XRD, Bruker D8 FOCUS 2200 V, with Cu Kα radiation and nickel as K_β filter). UV–Vis diffuse reflectance spectra were measured with Shimadzu UV-2600 using $BaSO_4$ powder as the reference sample. X-ray photoelectron spectra (XPS) were recorded by a UlVAC PHI-5000 VersaProbe instrument with monochromatic Al

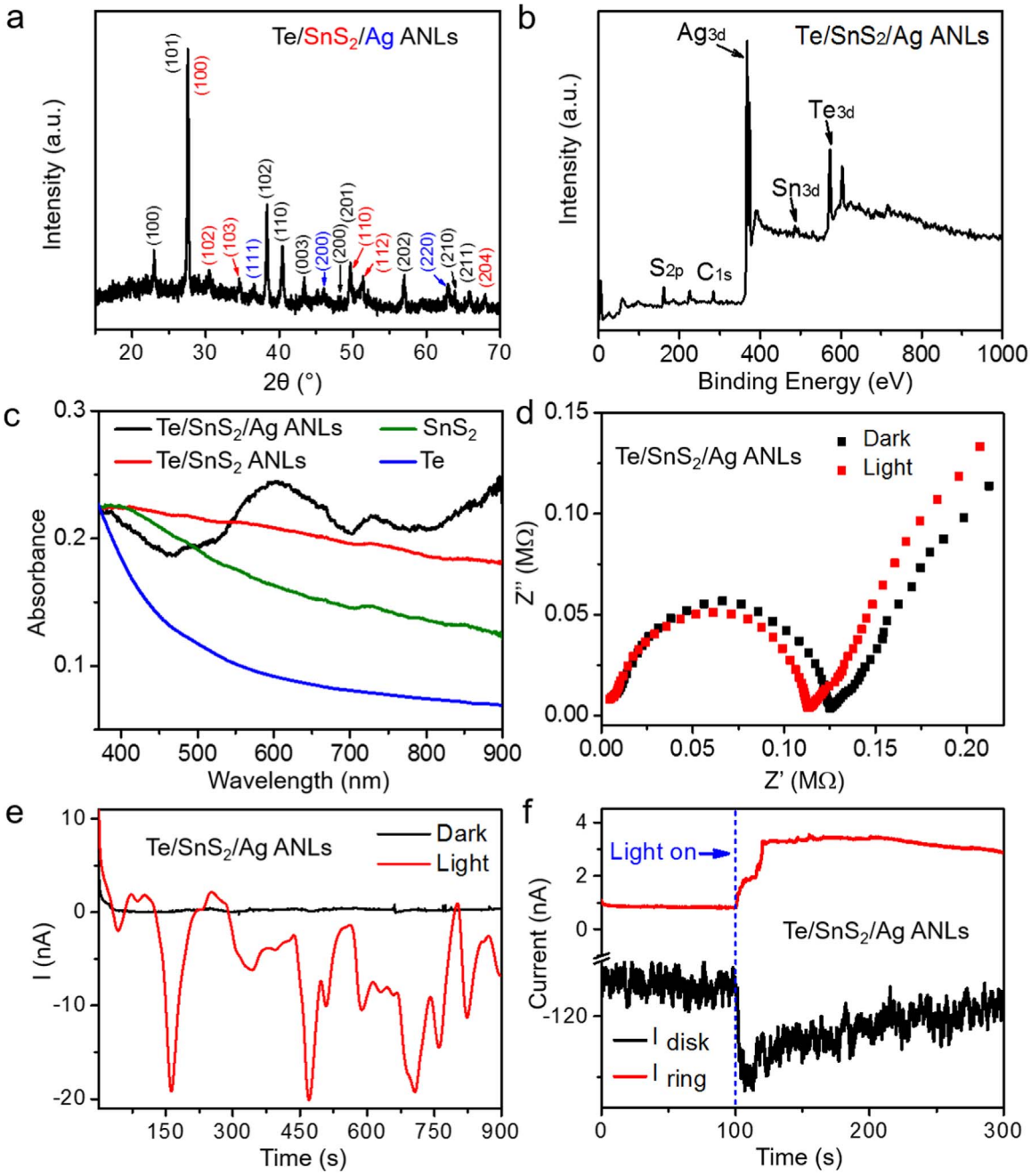

Fig. 3. (a) XRD and (b) XPS spectra of Te/SnS_2/Ag ANLs. (c) UV–Vis absorption of Te/SnS_2/Ag ANLs (black), Te/SnS_2 ANLs (red), Te nanowires (blue) and SnS_2 nanoplates (green), respectively. (d) EIS analysis and (e) current-time curves of Te/SnS_2/Ag ANLs measured with a standard three-electrode system in deionized water under dark and visible-light illumination, respectively. (f) Current-time curves of Te/SnS_2/Ag ANLs measured with RRDE (1600 rpm) in deionized water under visible-light illumination applied at the time of 100 s.

Kα X-ray radiation (1486.6 eV), and all binding energies were calibrated with the C1s peak at 284.6 eV. Specific surface area data were obtained through N_2 sorption at 77 K on a Quantachrome Autosorb IQ-2C instrument according to the Brunauer-Emmett-Teller (BET) model, all of the samples were degassed at 120 °C and 10^{-6} Torr for 5 h before the surface area measurements.

2.6. Electrochemical tests

The electrochemical impedance spectroscopy (EIS), rotating ring-disk electrode (RRDE) measurements and chronoamperometry analysis were carried out in the dark or under visible-light illumination with a standard three-electrode cell using a Chenhua CHI-760E electrochemical workstation. For preparing working electrodes, 5.0 mg of photocatalyst was dispersed in 50 mL of deionized water, and 5 μL of this suspension was uniformly coated on glass carbon rotating disk electrode (RDE, ALS Co., with a diameter of 5.0 mm and a rotating speed of 1600 rpm). A platinum wire was used as counter electrode, a saturated calomel electrode was used as reference electrode and deionized water was used as electrolyte. The electrochemical tests were performed under dark or visible-light irradiation (400–800 nm, 96 mW cm^{-2}), respectively.

2.7. Calculation of electron transfer numbers

To understand the electron-transfer process, RRDE experiments were also carried out in a standard three electrode system described in Section 2.6, except for the working electrode was RRDE. The

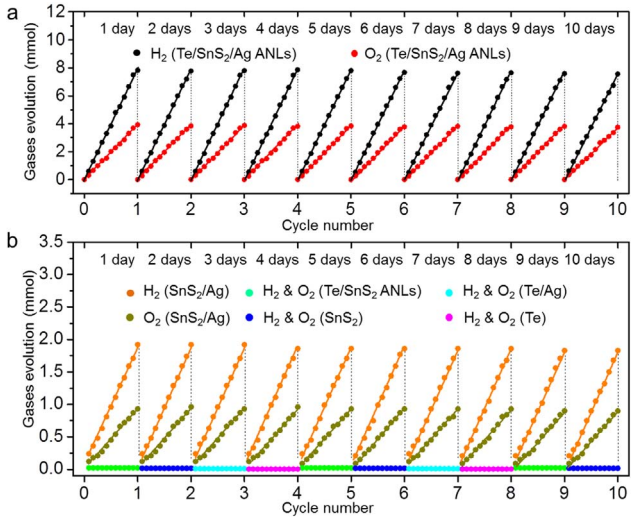

Fig. 4. (a,b) Gases evolution of Te/SnS_2/Ag ANLs and control samples under visible-light illumination in deionized water. The H_2 yield rate of Te/SnS_2/Ag ANLs and SnS_2/Ag was found to be 332.4 μmol h^{-1} and 80.1 μmol h^{-1}, respectively. No H_2 or O_2 generation was detected from Te/SnS_2 ANLs, Te/Ag, pristine Te nanowires and pristine SnS_2 nanoplates.

photocatalyst was applied on the RRDE working electrode with the same previously-mentioned procedure. The RRDE experiments were measured at open-circuit voltage with a rotation speed of 1600 rpm under dark and visible-light irradiation (400–800 nm, 96 mW cm^{-2}), respectively.

The electron transfer number was calculated according to the following equation:

$$n = \frac{4I_{disk}}{I_{disk} + I_{ring}/N} \quad (1)$$

where N is the collection efficiency of RRDE (0.424 in our system). The electron-transfer number was calculated to be 2.48 for Te/SnS_2/Ag ANLs, verifying that the water-splitting reaction was mainly carried out *via* a two-electron process with the intermediate product of H_2O_2. The oxidation reaction from H_2O to H_2O_2 is the rate-determining step, followed by rapid H_2O_2 adsorption and decomposition to H_2O and O_2.

2.8. Measurements of H_2 and O_2 generation rates

The photocatalytic water-splitting experiments were carried out in a top-irradiation quartz glass reaction vessel (360 mL) combing with a gas circulation vacuum system (CEL-SPH2N, CEAULIGHT). Typically, 300 mg of photocatalyst was mixed with 100 mL deionized water by ultrasonication in the quartz reaction vessel without adding any sacrificial reagent. The reaction vessel was evacuated to 1.0 kPa, and then the suspension was stirred vigorously and irradiated by a 300 W Xe lamp (205 mW cm^{-2}) with a designated filter. The UV light was provided by a UVREF filter (200–400 nm) and the visible light was provided by a VisREF filter (420–780 nm), respectively. Each cycle of photocatalytic water-splitting experiment lasted for 24 h. Before the next cycle, the reaction vessel was evacuated to the same vacuum state of 1.0 kPa. The temperature of reaction vessel was kept at 10 °C during the entire process. The amount of yielded H_2 and O_2 was evaluated using a calibrated gas chromatograph (GC7900, Shanghai Techcomp).

2.9. Measurement and calculation of STH efficiency of Te/SnS_2/Ag ANLs

Instead of 300 W Xe lamp, the STH efficiency of Te/SnS_2/Ag ANLs was investigated under full-spectrum AM 1.5G solar illumination (100 mW cm^{-2}) provided by a SXDN-150E solar simulator. All other experimental conditions were the same as those in Section 2.8. The total incident power over the 20.0 cm^2 irradiated area of reaction vessel was 2.0 W, so the total input energy over 12.0 h was E_{solar} = 2.0 × 3600 × 12.0 J = 86.4 kJ.

After 12.0 h of continuous illumination, an average amount of 1.8 mmol H_2 was collected and detected by gas chromatography, which revealed that the energy stored in H_2 generated by photocatalytic water-splitting is $E_{H2} = 1.8 \times 10^{-3} \times 6.02 \times 10^{23} \times 2.46 \times 1.609 \times 10^{-19}$ J = 0.43 kJ, where 2.46 eV is the free energy of water splitting.

Therefore, The STH efficiency can be calculated as: $\eta_{STH} = E_{H2}/E_{solar}$ = 0.43 kJ/86.4 kJ = 0.50%, assuming all incident light was optically absorbed by the Te/SnS_2/Ag ANLs suspended in pure water.

3. Results and discussion

The method for preparing Te/SnS_2/Ag ANLs was detailed in the Supporting information. Similar to the structure of tree leaves offered in Fig. 1a, the Te nanowire served as the branch of Te/SnS_2/Ag ANLs to string together all the SnS_2 nanoplates with Ag nanoparticles decorated on the surface, as presented by scanning electron microscopy (SEM) images (Fig. 1b,c and Fig. S1). The average diameter and length of Te/SnS_2/Ag ANLs is measured to be 180 nm and 10 μm, respectively. Fig. 1d-g and Fig. S2a-c show the uniform morphology and features of Te/SnS_2/Ag ANLs. It can be observed that only a small number of Te nanowires are not completely covered by SnS_2 nanoplates. The corresponding EDS mappings of Fig. S2c are shown in Fig. S2d-f, clearly presenting the distribution of Te, Sn and S elements in the Te/SnS_2/Ag ANLs.

To investigate the relation between structural characteristics and photocatalytic performances, various control samples, including pristine Te nanowires (Fig. S3), pristine SnS_2 nanoplates (Fig. S4 and S5), Te nanowires decorated with Ag nanoparticles (Te/Ag), SnS_2 nanoplates decorated with Ag nanoparticles (SnS_2/Ag), and Te/SnS_2 ANLs without decorated Ag nanoparticles were also prepared and tested.

Structural characterizations of Te/SnS_2/Ag ANLs were performed by transmission electron microscopy (TEM). Fig. 2a shows several Te/SnS_2/Ag ANLs randomly dispersed on TEM grid. Magnified TEM image of Te/SnS_2/Ag ANLs (Fig. 2b) exhibits numerous well-dispersed Ag nanoparticles attached on SnS_2 nanoplates. High-resolution TEM (HRTEM) image of a Te nanowire in Te/SnS_2/Ag ANLs reveals a 0.310 nm d-spacing (Fig. 2c), consistent with the Te (101) crystalline planes. The high crystallinity of Te nanowires was further confirmed (Fig. S3), which is beneficial to charge transport. Fig. 2d shows a HRTEM image and corresponding selected-area electron diffraction (SAED) pattern of SnS_2 nanoplate in Te/SnS_2/Ag ANLs, the lattice spacing is 0.316 nm, identical to the (100) crystalline planes of hexagonal SnS_2. Further HRTEM characterizations confirm the SnS_2 nanoplates were grown on the surface of Te nanowires (Fig. S6). HRTEM images show Ag nanoparticles and concomitantly-formed Ag_2S nanodots on SnS_2 nanoplates (Fig. 2e,f), the d-spacings of 0.237 nm and 0.30 nm are in line with Ag (111) and Ag_2S (111) lattice planes. The formation of a small amount of Ag_2S along was ascribed to the side reaction of $AgNO_3$ with SnS_2 nanoplates during the photo-deposition/decoration process of Ag nanoparticles.

The high crystallinity of Te/SnS_2/Ag ANLs was further confirmed by the strong diffraction peaks in X-ray diffraction (XRD) spectrum, as shown in Fig. 3a. The peaks marked with black, red and blue colors were indexed to hexagonal Te (JCPDS no. 36-1452), hexagonal SnS_2 (JCPDS no. 23-677) and face-centered-cubic Ag (JCPDS no. 04-0783), respectively. The specific surface area of Te/SnS_2/Ag ANLs was measured to be ~ 33.4 $m^2 g^{-1}$ (Fig. S7). X-ray photoelectron spectroscopy (XPS) revealed the existence of Te, SnS_2, Ag and Ag_2S in Te/SnS_2/Ag ANLs (Fig. 3b and Fig. S8). UV–Vis absorption spectra of Te/SnS_2/Ag ANLs and control samples (such as Te/SnS_2 ANLs, pristine Te nanowires and pristine SnS_2 nanoplates) were collected, respectively (Fig. 3c). Through UV–Vis diffuse reflectance spectroscopy, the bandgap of Te nanowires and SnS_2 nanoplates were determined to be 0.75 and 2.20 eV, respectively (Fig. S9). Notably, Te/SnS_2/Ag ANLs exhibit

much stronger visible-light absorption than that of Te/SnS_2 ANLs, owing to the SPR effect of decorated Ag nanoparticles [22]. Moreover, the Raman peak intensities of Te/SnS_2/Ag ANLs also show an obvious enhancement compared to those of Te/SnS_2 ANLs without decorating Ag nanoparticles (Fig. S10), demonstrating the surface enhanced Raman scattering (SERS) originated from Ag nanoparticles [23].

The electrochemical impedance spectra (EIS) of Te/SnS_2/Ag ANLs and control samples under dark and visible-light illumination are shown in Fig. 3d and Fig. S11, respectively. The conductivity of Te/SnS_2/Ag ANLs clearly increased under visible light, confirming the generation of more charge carriers upon illumination. The current oscillations in the current-time curves of Te/SnS_2/Ag ANLs under visible-light illumination (Fig. 3e) indicate the cycles of H_2O_2 generation, adsorption and decomposition. The visible-light-driven photocatalytic reactions on Te/SnS_2/Ag ANLs can be mainly described as the following stepwise two-electron process [11]:

$$hv \rightarrow e^- + h^+ \quad (2)$$

$$2H_2O + 2h^+ \leftrightarrow H_2O_2 + 2H^+ \quad (3)$$

$$2H_2O_2 \rightarrow 2H_2O + O_2 \quad (4)$$

$$2H^+ + 2e^- H_2 \quad (5)$$

The strong current oscillation exhibited by Te/SnS_2/Ag ANLs, indicating the fast H_2O_2 generation and the decomposition of H_2O_2 to H_2O and O_2. Pristine SnS_2 nanoplates and Te/SnS_2 ANLs also show similar cycles but with much lower current intensity (Fig. S12); however, no O_2 generation was detected on pristine SnS_2 nanoplates and Te/SnS_2 ANLs, owing to the reverse reaction of H_2O_2 to water, as indicated in Eq. (3). The electron-transfer number of Te/SnS_2/Ag ANLs measured with rotating ring-disk electrode (RRDE) under visible-light illumination was calculated to be 2.48 (Fig. 3f, as detailed in Section 2), further verifying that the water-splitting process was mainly carried out *via* the above two-electron process with H_2O_2 as intermediate product (Scheme 1b).

The H_2 generation rate of Te/SnS_2/Ag ANLs was measured to be 332.4 μmol h^{-1}, which is ~ 4 times higher than that of SnS_2/Ag (80.1 μmol h^{-1}). The solar-to-hydrogen (STH) efficiency of Te/SnS_2/Ag ANLs under visible light was measured using a solar simulator (through a VisREF filter, 420–780 nm) and calculated to be 0.50% following a previous method [11] (as detailed in Section 2), exhibiting remarkable photocatalytic performance compared to other existing photocatalysts (as detailed in Table S1, Supporting information). The long-term stability was investigated by testing under visible light for 10 cycles (24 h per cycle, see Fig. 4). Both Te/SnS_2/Ag ANLs and SnS_2/Ag maintained high sustainability for H_2 and O_2 generation. The SEM images of Te/SnS_2/Ag ANLs after testing for 240 h (Fig. S13) reveal the high structural integrity and stability. As shown in Fig. S14, the high-resolution XPS spectra at Sn 3d and S 2p regions of Te/SnS_2/Ag ANLs were measured after photocatalytic testing for 240 h to confirm the stability. The two characteristic peaks of SnS_2 centered at 486.3 eV (Sn $3d_{5/2}$) and 495.0 eV (Sn $3d_{3/2}$) remained unchanged, and the main doublet of S $2p_{3/2}$ and S $2p_{1/2}$ peaks centered at 161.9 and 163.1 eV showed no change. Moreover, the oxidation peak at binding energy of 168.8 eV derived from SO_4^{2-} is absent, further ruling out the surface oxidation of Te/SnS_2/Ag [24,25]. In contrast, no detectable H_2 or O_2 generation was observed from Te/SnS_2 ANLs, which might be caused by the high recombination rate of photogenerated electrons and holes. These results indicate that Ag nanoparticles play a key role as crucial co-catalyst for overall splitting of pure water [26]. Additionally, no H_2 or O_2 generation was observed from Te/Ag, pristine SnS_2 nanoplates and pristine Te nanowires, mainly due to the inappropriate band structures and fast recombination of electron-hole pairs.

Moreover, when exposed under ultraviolet illumination by applying a UVREF filter (200–400 nm), Te/SnS_2/Ag ANLs and all the control samples show no H_2 or O_2 evolution. We also tested the performance of commercially-available plantinized-TiO_2 (P25), which only achieved a H_2 production rate of 31.8 μmol·h^{-1} (and no O_2 evolution) under full-spectrum light with the assistance of H_2PtCl_6 (0.1 wt% per TiO_2) and 2 wt% methanol as sacrificial reagents. The results show the water-splitting capability of Te/SnS_2/Ag ANLs is far superior to that of P25.

The greatly-enhanced overall water-splitting efficiency of Te/SnS_2/Ag ANLs can be ascribed to the following factors: 1) The n-type SnS_2 nanoplates with ultrathin thickness, high crystallinity, suitable band gap (E_g = 2.2 eV, as shown in Fig. S9) and preferable edge-state position [20,21] guaranteed strong light absorption and charge generation. The redox potential of H_2O sandwiched between the conduction band and valence band of SnS_2 meets the requirement for photocatalytic water-splitting. 2) The Ag nanoparticles decorated on ANLs served as excellent electron collector and sources of localized SPR [18,22,27–29]. The decoration of Ag nanoparticles is the key factor for the H_2 evolution of Te/SnS_2/Ag ANLs and SnS_2/Ag. Moreover, the concomitantly-formed Ag_2S nanodots on the SnS_2 nanoplate is highly conductive to facilitate charge transfer for interfacial water-splitting reaction, benefited from the chemical bonding of Sn-S-Ag-S [30]. 3) Highly-conductive p-type Te nanowires contributed to the charge separation (especially the transport of holes) and transfer kinetics [19,31], thus resulting in greatly improved STH efficiency of Te/SnS_2/Ag ANLs compared to that of SnS_2/Ag. The well-defined interface of Te/SnS_2 p-n junctions may also help to improve the charge separation/transport properties [32–34]. Additionally, the good hydrophilicity and dispersibility of Te/SnS_2/Ag ANLs in water could also be a favorable factor [35–37]. In brief, the rational design of unique “artificial nanoleaves” architecture ensured strong light absorption and provided a highway for smooth charge migration to the photocatalyst/water interface where the water-splitting reaction occurred (Scheme 1).

4. Conclusion

In summary, an efficient and stable photocatalyst for overall water-splitting without the need of any sacrificial reagent is developed by rational design and assembly of different functional nanostructures together. The synergistic effect in Te/SnS_2/Ag ANLs made of three carefully-selected components and architectures promoted light absorption, electron-hole pair separation and surface redox reaction, thus enabled simultaneous H_2 and O_2 generation with greatly enhanced STH efficiency.

Acknowledgements

This work was supported by National Key Research and Development Program of China (2017YFA0208200, 2016YFB0700600), National Key Basic Research Program (2015CB659300), Projects of NSFC (21403105, 21573108), Fundamental Research Funds for the Central Universities (020514380107), and a project funded by the Priority Academic Program Development of Jiangsu Higher Education Institutions.

Appendix A. Supporting information

Supplementary data associated with this article can be found in the online version at http://dx.doi.org/10.1016/j.nanoen.2017.07.039.

References

[1] A. Kudo, Y. Miseki, Chem. Soc. Rev. 38 (2009) 253–278.
[2] F.E. Osterloh, Chem. Soc. Rev. 42 (2013) 2294–2320.
[3] X.B. Chen, S.H. Shen, L.J. Guo, S.S. Mao, Chem. Rev. 110 (2010) 6503–6570.
[4] S.U.M. Khan, M. Al-Shahry, W.B. Ingler, Science 297 (2002) 2243–2245.
[5] R. Asahi, T. Morikawa, T. Ohwaki, K. Aoki, Y. Taga, Science 293 (2001) 269–271.
[6] D.P. Cao, W.J. Luo, J.Y. Feng, X. Zhao, Z.S. Li, Z.G. Zou, Energy Environ. Sci. 7 (2014) 752–759.
[7] T.K. Townsend, E.M. Sabio, N.D. Browning, F.E. Osterloh, Energy Environ. Sci. 4

(2011) 4270–4275.
[8] Q. Li, B.D. Guo, J.G. Yu, J.R. Ran, B.H. Zhang, H.J. Yan, J.R. Gong, J. Am. Chem. Soc. 133 (2011) 10878–10884.
[9] J.H. Yang, D.G. Wang, H.X. Han, C. Li, Acc. Chem. Res. 46 (2013) 1900–1909.
[10] S.B. Yang, Y.J. Gong, J.S. Zhang, L. Zhan, L.L. Ma, Z.Y. Fang, R. Vajtai, X.C. Wang, P.M. Ajayan, Adv. Mater. 25 (2013) 2452–2456.
[11] J. Liu, Y. Liu, N.Y. Liu, Y.Z. Han, X. Zhang, H. Huang, Y. Lifshitz, S.T. Lee, J. Zhong, Z.H. Kang, Science 347 (2015) 970–974.
[12] Y.C. Qiu, K.Y. Yan, H. Deng, S.H. Yang, Nano Lett. 12 (2012) 407–413.
[13] J.H. Park, S. Kim, A.J. Bard, Nano Lett. 6 (2006) 24–28.
[14] Z.Y. Yin, Z. Wang, Y.P. Du, X.Y. Qi, Y.Z. Huang, C. Xue, H. Zhang, Adv. Mater. 24 (2012) 5374–5378.
[15] M.R. Gao, Y.F. Xu, J. Jiang, S.H. Yu, Chem. Soc. Rev. 42 (2013) 2986–3017.
[16] W.J. Youngblood, S.H.A. Lee, K. Maeda, T.E. Mallouk, Acc. Chem. Res. 42 (2009) 1966–1973.
[17] S. Linic, P. Christopher, D.B. Ingram, Nat. Mater. 10 (2011) 911–921.
[18] H. Tong, S.X. Ouyang, Y.P. Bi, N. Umezawa, M. Oshikiri, J.H. Ye, Adv. Mater. 24 (2012) 229–251.
[19] G.D. Moon, SKo, Y.N. Xia, U. Jeong, ACS Nano 4 (2010) 2307–2319.
[20] M. Gratzel, Nature 414 (2001) 338–344.
[21] Y.F. Sun, H. Cheng, S. Gao, Z.H. Sun, Q.H. Liu, Q. Liu, F.C. Lei, T. Yao, J.F. He, S.Q. Wei, Y. Xie, Angew. Chem. Int. Ed. 51 (2012) 8727–8731.
[22] Z.W. Liu, W.B. Hou, P. Pavaskar, M. Aykol, S.B. Cronin, Nano Lett. 11 (2011) 1111–1116.
[23] J.A. Creighton, C.G. Blatchford, M.G. Albrecht, J. Chem. Soc. Faraday Trans. 75 (1979) 790–798.
[24] J.G. Wang, X.R. Li, J. Zhu, H.X. Li, Nanoscale 5 (2013) 1876–1881.
[25] L.B. Ma, Y. Hu, G.Y. Zhu, R.P. Chen, T. Chen, H.L. Lv, Y.R. Wang, J. Liang, H.X. Liu, C.Z. Yan, Z.X. Tie, Z. Jin, J. Liu, Chem. Mater. 28 (2016) 5733–5742.
[26] Z. Pan, Y. Zheng, F. Guo, P. Niu, X. Wang, ChemSusChem 10 (2017) 87–90.
[27] J. Turner, Nat. Mater. 7 (2008) 770–771.
[28] X.H. Li, M. Antonietti, Chem. Soc. Rev. 42 (2013) 6593–6604.
[29] Z.H. Xue, H. Su, Q.Y. Yu, B. Zhang, H.H. Wang, X.H. Li, J.S. Chen, Adv. Energy Mater. (2017) 1602355.
[30] Z. Li, S. Xiong, G. Wang, Z. Xie, Z. Zhang, Sci. Rep. 6 (2016) 19754.
[31] J.Q. Hu, A.L. Liu, H.L. Jin, D.K. Ma, D.W. Yin, P.S. Ling, S. Wang, Z.Q. Lin, J.C. Wang, J. Am. Chem. Soc. 137 (2015) 11004–11010.
[32] Y.P. Yuan, L.W. Ruan, J. Barber, S.C.J. Loo, C. Xue, Energ. Environ. Sci. 7 (2014) 3934–3951.
[33] T.N. Ye, L.B. Lv, M. Xu, B. Zhang, K.X. Wang, J. Su, X.H. Li, J.S. Chen, Nano Energy 15 (2015) 335–342.
[34] T.N. Ye, L.B. Lv, X.H. Li, M. Xu, J.S. Chen, Angew. Chem. Int. Ed. 53 (2014) 6905–6909.
[35] Z. Wang, J. Li, X. Tian, X. Wang, Y. Yu, K.A. Owusu, L. He, L. Mai, ACS Appl. Mater. Interfaces 8 (2016) 19386–19392.
[36] Y. Zhao, L. Xu, L. Mai, C. Han, Q. An, X. Xu, X. Liu, Q. Zhang, PNAS 109 (2012) 19569–19574.
[37] H. Wang, H.W. Lee, Y. Deng, Z. Lu, P.C. Hsu, Y. Lin, D. Liu, Y. Cui, Nat. Commun. 6 (2015) 7261.